ARL-MR-1088 ● Oct 2023

Multi-fidelity Data Fusion for Aerodynamic Prediction Including Parametric Uncertainty

by Bradley T Burchett

NOTICES

Disclaimers

The findings in this report are not to be construed as an official Department of the Army position unless so designated by other authorized documents.

Citation of manufacturer's or trade names does not constitute an official endorsement or approval of the use thereof.

Destroy this report when it is no longer needed. Do not return it to the originator.

ARL-MR-1088 ● OCT 2023

Multi-fidelity Data Fusion for Aerodynamic Prediction Including Parametric Uncertainty

Bradley T Burchett
DEVCOM Army Research Laboratory

REPORT DOCUMENTATION PAGE

1. REPORT DATE	2. REPORT TYPE	3. DATES COVERED	
		START DATE	END DATE
October 2023	Memorandum Report	4/01/2023	8/24/2023

4. TITLE AND SUBTITLE
Multi-fidelity Data Fusion for Aerodynamic Prediction Including Parametric Uncertainty

5a. CONTRACT NUMBER	5b. GRANT NUMBER	5c. PROGRAM ELEMENT NUMBER
5d. PROJECT NUMBER	**5e. TASK NUMBER**	**5f. WORK UNIT NUMBER**

6. AUTHOR(S)
Bradley T Burchett

7. PERFORMING ORGANIZATION NAME(S) AND ADDRESS(ES)	8. PERFORMING ORGANIZATION REPORT NUMBER
DEVCOM Army Research Laboratory ATTN: FCDD-RLA-WD Aberdeen Proving Ground, MD 21005	ARL-MR-1088

9. SPONSORING/MONITORING AGENCY NAME(S) AND ADDRESS(ES)	10. SPONSOR/MONITOR'S ACRONYM(S)	11. SPONSOR/MONITOR'S REPORT NUMBER(S)

12. DISTRIBUTION/AVAILABILITY STATEMENT
DISTRIBUTION STATEMENT A. Approved for public release: distribution unlimited.

13. SUPPLEMENTARY NOTES
ORCID ID: Bradley T Burchett, 0000-0002-1934-0537

14. ABSTRACT
Recent developments in data fusion provide an algorithmic means of combining predictions from models of various fidelities into a unified model that provides both the mean and variance of desired outputs over the input space. In this work we show how cokriging can be used to combine aerodynamic predictions from four data sources into a single Gaussian process (GP) regression model. We use the multi-fidelity Gaussian utilities from the Sora flight prediction tool from Lawrence Livermore National Laboratory to perform cokriging and interpolation of total force and moment coefficients as functions of Mach, angle of attack (AoA), and aerodynamic bank angle. We use generalized least squares (LS) regression to convert the total force and moment predictions to polynomials with the sine of AoA as the variable. By propagating the uncertainty from GP predictions through the LS regression, we can choose a polynomial form with minimal coefficient uncertainty. The final model form consists of tables of polynomial coefficients as functions of Mach and aerodynamic bank angle.

15. SUBJECT TERMS
spark range, projectile aerodynamics, trajectory reconstruction, system identification, Weapons Sciences

16. SECURITY CLASSIFICATION OF:			17. LIMITATION OF ABSTRACT	18. NUMBER OF PAGES
a. REPORT	b. ABSTRACT	C. THIS PAGE		
UNCLASSIFIED	UNCLASSIFIED	UNCLASSIFIED	UU	35

19a. NAME OF RESPONSIBLE PERSON	19b. PHONE NUMBER *(Include area code)*
Bradley T Burchett	(410) 306-0792

STANDARD FORM 298 (REV. 5/2020)
Prescribed by ANSI Std. Z39.18

Contents

List of Figures

Acknowledgments

The author wishes to thank the Flight Performance Integration team at Lawrence Livermore National Laboratory, especially D Driver and J Movva, for their tireless efforts both configuring the software for use and introducing the author to its operation.

1. Introduction

Aerodynamic prediction has been an active field of research for many decades. Now with the ubiquity of computational fluid dynamics (CFD), high-fidelity predictions can be rendered with little to no dependence on wind tunnel tests. CFD methods can provide several levels of prediction fidelity depending on the particular code used, mesh density, and modeling assumptions (inviscid, Reynolds Averaged Navier-Stokes [NS], etc.). Current computer applications can be categorized roughly as three levels of prediction fidelity—semi-empirical, inviscid CFD, and NS CFD. We have listed these from lowest to highest fidelity. Wind tunnel tests are time consuming and expensive in comparison to computer simulations but are indisputably the nearest to "truth" apart from actual flight tests. Thus, in the best case, aerodynamic predictions for a particular configuration can be rendered at four or more levels of fidelity. The cost required to make a prediction using a particular model is inversely proportional to its fidelity. That is, the higher fidelity, the greater the cost in computational effort or experimental man-hours.

Data fusion describes the process of combining predictions from models of varying fidelity into a unified, superior model. Ideally, data fusion provides a model with the best prediction over a large input space while inquiring of precursor models in an optimal way. In the best case, a data fusion approach would use many inquiries of the lower-fidelity models and very few of the highest-fidelity model to produce a model that predicts the relevant outputs with very little uncertainty.

Over the past two decades, kriging methods have become the aerospace industry standard in aerodynamic data fusion. Kriging originated in the mining community[1] and was recently adopted by the computer science community.[2] The aerospace community now uses cokriging[3] or one of its variants[4] at the exclusion of previous methods.

In this report, we show how cokriging can be used to combine four large sets of predictions for an axisymmetric missile[5–7] into a single model. The resulting model provides predictions of mean and variance for total force and moment vectors in 3-D. We use generalized least-squares regression to convert the total force-moment predictions to polynomials with sine of angle of attack (AoA) as the variable. Generalized least squares propagates prediction uncertainty through the regression so the analyst can choose a polynomial order such that coefficient uncertainties are minimized. The final model consists of tables of polynomial coefficients as functions of Mach and aerodynamic bank angle and includes uncertainty on each coefficient.

2. Kriging and Cokriging

2.1 Kriging

Kriging is a statistical interpolation method introduced first in the mining community by Krige.[1] It has come into recent prominence in the aerodynamic modeling and aerospace multidisciplinary design communities. One of the most accessible treatments of kriging and cokriging is by Forrester et al.[2] We rely on their notation here as modified by Bailly and Bailly.[3] Kriging is closely related to the radial basis function in machine learning and relies on spatial correlation between n sample points $(\boldsymbol{X_1}, \ldots, \boldsymbol{X_n})$, for which the function values have been found $(\boldsymbol{Y_1}, \ldots, \boldsymbol{Y_n})$. The kriging model is a Gaussian process (GP) with covariance given as

$$\mathbf{Cov}\left(\boldsymbol{X_i}, \boldsymbol{X_j}\right) = \sigma^2 \boldsymbol{R}\left(\boldsymbol{X_i}, \boldsymbol{X_j}: \boldsymbol{\theta}\right) + \mathbf{gI}\left(\boldsymbol{X_i}, \boldsymbol{X_j}\right) \tag{1}$$

where σ^2 is the variance of the process, and $\boldsymbol{R}$ is a correlation function with hyperparameters $\boldsymbol{\theta}$. The results shown in this paper use the Matern 5/2 kernel.[8,9]

$$\boldsymbol{R}\left(\boldsymbol{X_i}, \boldsymbol{X_j}: \boldsymbol{\theta}\right) = \left(1 + \frac{\sqrt{5}\left|\boldsymbol{X_i} - \boldsymbol{X_j}\right|}{\boldsymbol{\theta}} + \frac{5\left|\boldsymbol{X_i} - \boldsymbol{X_j}\right|^2}{3\boldsymbol{\theta}^2}\right) \cdot \exp\left(-\sqrt{5}\left|\boldsymbol{X_i} - \boldsymbol{X_j}\right|/\boldsymbol{\theta}\right) \tag{2}$$

where $\boldsymbol{\theta^2}$ is the variance, $\boldsymbol{R}\left(\boldsymbol{X_i}, \boldsymbol{X_j}: \boldsymbol{\theta}\right) \leq 1, \forall\ (i, j)$. The hyperparameters consist of $(\boldsymbol{\theta}, \boldsymbol{g})$, which may both have differing values in each dimension. They are found by maximizing the likelihood function

$$L = -\frac{N}{2}\ln(\sigma^2) - \frac{1}{2}\ln(\det(\boldsymbol{R})) \tag{3}$$

We use a maximum likelihood estimation to determine the set of best $\boldsymbol{\theta}, \boldsymbol{g}$ for each surface representing a particular force/moment coefficient.[8]

The kriging prediction is the unbiased maximum likelihood estimate given by

$$\hat{Y}(\boldsymbol{X}) = \mu_Y + \boldsymbol{r}^{\mathrm{T}}(\boldsymbol{X})\boldsymbol{R}^{-1}(\boldsymbol{Y_c} - \mathbf{1}\mu_Y) \tag{4}$$

where $\boldsymbol{r}(\boldsymbol{X}) = \boldsymbol{R}\left(\boldsymbol{X}, \boldsymbol{X_j}: \boldsymbol{\theta}\right), j = 1, \ldots, n$, that is, a column vector, $\mu_Y = \mathbf{1}^T\boldsymbol{R}^{-1}\boldsymbol{Y_c}/(\mathbf{1}^T\boldsymbol{R}^{-1}\mathbf{1})$, and $\mathbf{1}$ is an $n \times 1$ column vector of ones.

2.2 Cokriging

Cokriging is a well-established method to increase the fidelity of a low-cost predictor by adjusting its output to match a sparse set of high-fidelity predictions. The general idea is that the high cost predictions can be modeled by scaling the low cost predictions by a factor ρ and adding a second GP $\boldsymbol{Z_d}$.

$$\boldsymbol{Z}_e(\boldsymbol{X}) = \rho \boldsymbol{Z}_c(\boldsymbol{X}) + \boldsymbol{Z}_d(\boldsymbol{X}) \tag{5}$$

To find the second model there must be some overlap in the underlying data sets and typically $\boldsymbol{X_e} \subset \boldsymbol{X_c}$. A combined covariance matrix is built as:

$$\boldsymbol{C}(\boldsymbol{X_c}, \boldsymbol{X_e}: \boldsymbol{\theta_c}, \boldsymbol{\theta_d}) = \begin{bmatrix} \sigma_c^2 \boldsymbol{R_c}(\boldsymbol{X_c}, \boldsymbol{X_c}) & \rho\sigma_c^2 \boldsymbol{R_c}(\boldsymbol{X_c}, \boldsymbol{X_e}) \\ \rho\sigma_c^2 \boldsymbol{R_c}(\boldsymbol{X_e}, \boldsymbol{X_c}) & \rho^2\sigma_c^2 \boldsymbol{R_c}(\boldsymbol{X_e}, \boldsymbol{X_e}) + \sigma_d^2 \boldsymbol{R_d}(\boldsymbol{X_e}, \boldsymbol{X_e}) \end{bmatrix} \tag{6}$$

where the subscripts (c, d) indicate which set of hyperparameters are used to form that particular quantity. The low-fidelity hyperparameters are found by kriging the low-fidelity data as shown in Section 2.1. To determine the hyperparameters for the high-fidelity set, difference data is found from the overlapping samples.

$$\boldsymbol{d} = \boldsymbol{y}_e - \rho \boldsymbol{y}_c(\boldsymbol{X_e}) \tag{7}$$

And maximizing the updated likelihood function

$$L = -\frac{N_e}{2}\ln(\sigma_d^2) - \frac{1}{2}\ln(\det(\boldsymbol{R_d}(\boldsymbol{X_e}, \boldsymbol{X_e}))) \tag{8}$$

The cokriging maximum likelihood predictor is then given by:

$$\hat{Y}_e(\boldsymbol{X}) = \mu_Y + \boldsymbol{c}^{\mathrm{T}}(\boldsymbol{X})\boldsymbol{C}^{-1}(\boldsymbol{Y} - \boldsymbol{1}\mu_Y) \tag{9}$$

with a variance of

$$s^2(\boldsymbol{X}) = \hat{\rho}^2\hat{\sigma}_c^2 + \hat{\sigma}_d^2 - \boldsymbol{c}^T(\boldsymbol{X})\boldsymbol{C}^{-1}\boldsymbol{c}(\boldsymbol{X}) \tag{10}$$

where

$$\mathbf{c} = \begin{bmatrix} \rho\sigma_c^2 R(\boldsymbol{X}, \boldsymbol{X_c}: \boldsymbol{\theta_c}) \\ \rho^2\sigma_c^2 R(\boldsymbol{X}, \boldsymbol{X_e}: \boldsymbol{\theta_c}) + \sigma_d^2 R(\boldsymbol{X}, \boldsymbol{X_e}: \boldsymbol{\theta_d}) \end{bmatrix} \tag{11}$$

and $\boldsymbol{Y} = [\boldsymbol{Y_c^T} \quad \boldsymbol{Y_e^T}]^{\boldsymbol{T}}$, $\mu_Y = \boldsymbol{1}^T\boldsymbol{C}^{-1}\boldsymbol{Y}/(\boldsymbol{1}^T\boldsymbol{C}^{-1}\boldsymbol{1})$

For this work, cokriging was performed using the Lawrence Livermore National Laboratory's Sora tool.[8,9] Sora's multi-fidelity cokriging utility will form a GP model from up to three multi-fidelity data sources at once.

3. Generalized Least Squares (lscov.m)

The final aerodynamic model will use polynomials rather than the GP surrogates. A typical polynomial model has the form:

$$y = \beta_0 x_0 + \beta_1 x_1 + \beta_2 x_2 + \cdots + \beta_m \cdot x_m \tag{12}$$

where $\beta_0, \ldots, \beta_{m-1}$ are unknown constants, and $x_0, \ldots, x_m$ are the regressors. Given the model of Eq. 11 and data vector $\mathbf{y}$ of length > m, and matrix of regressors X, the least squares estimate for the coefficient vector $\boldsymbol{\beta} = [\beta_0, \beta_1, \beta_2, \ldots, \beta_m]$ can be found by[9]

$$\boldsymbol{\beta} = (\mathbf{X}^T\mathbf{X})^{-1}(\mathbf{X}^T\mathbf{y}) \tag{13}$$

For our application, the regressors will be $x_i = \sin^i \bar{\alpha}$, and the constants will be tabulated as functions of Mach and aerodynamic bank angle, $\beta_i = \beta_i(M, \phi)$.

Since the cokriging/GP model provides both the mean and variance at each sample point, these variances can be propagated through generalized least squares to estimate the variance on each constant $\beta_i(M, \phi)$.[10]

Thus, we want the best estimate of $\boldsymbol{\beta}$ such that $\|\mathbf{X}\boldsymbol{\beta} - \mathbf{y}\|_2$ is minimized. When the observations y have known covariances $\mathbf{V}$, we must instead minimize the weighted squares $(\mathbf{X}\boldsymbol{\beta} - \mathbf{y})^T\mathbf{V}^{-1}(\mathbf{X}\boldsymbol{\beta} - \mathbf{y})$. This leads to the following formulae.

$$\boldsymbol{\beta} = (\mathbf{X}^T\mathbf{V}^{-1}\mathbf{X})^{-1}(\mathbf{X}^T\mathbf{V}^{-1}\mathbf{y}) \tag{14}$$

$$\mathbf{mse} = \mathbf{y}^T(\mathbf{V}^{-1} - \mathbf{V}^{-1}\mathbf{X}(\mathbf{X}^T\mathbf{V}^{-1}\mathbf{X})^{-1}\mathbf{X}^T\mathbf{V}^{-1})\mathbf{y}/(m-n) \tag{15}$$

$$\mathbf{S} = (\mathbf{X}^T\mathbf{V}^{-1}\mathbf{X})^{-1} \cdot \mathbf{mse} \tag{16}$$

And **S** is the covariance of the parameter estimates **β.**

4. Data Sources

We applied the methods described previously to a large data set for a generic tail-controlled symmetric projectile. Table 1 and Fig. 1 present the projectile characteristics. It is a finned projectile with long strakes to enhance lift and four trailing-edge mounted flaps that are independently controlled. The vehicle is expected to fly roll stabilized in one of two symmetric attitudes: "X" mode where the four strakes form an X when viewed from the tail, and "Plus" mode where two

strakes lie in the vertical plane and two lie in the horizontal. Positive flap deflections with the vehicle in "X" mode are denoted in Fig. 1b.

Diameter (mm)	Length-to-diameter	Length of ogive (cal.)	Root fin chord (cal.)	Tip fin chord (cal.)	Fin span (cal.)
105	10	3.0	6	2.2	1.935

Table 1 Parameters of the generic high-speed projectile

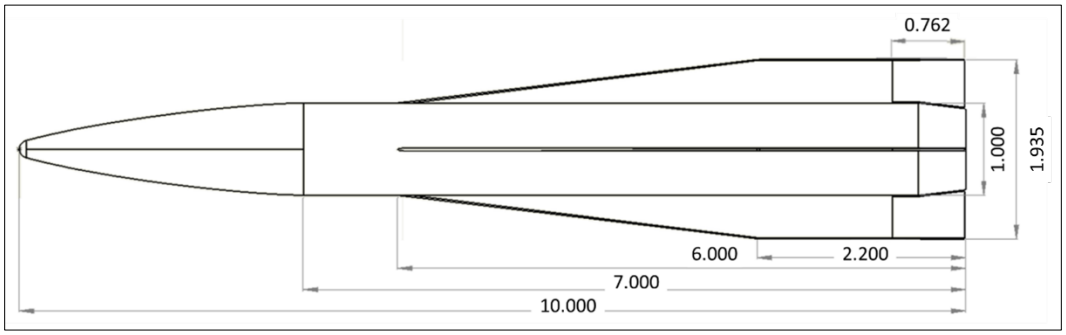

a) Generic high-speed projectile geometry (dimensioned in calibers)

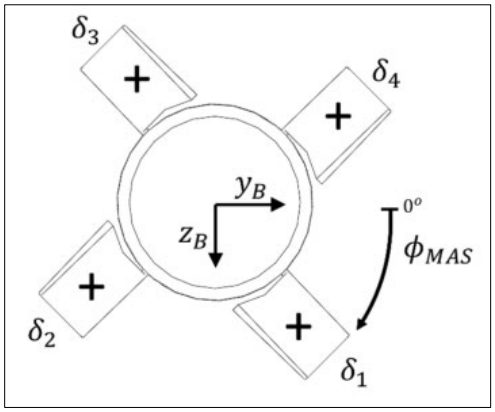

b) Positive flap deflection convention

Fig. 1 Generic high-speed projectile

Previous studies showed that the total forces and moments for any set of flap deflections can be found by applying superposition of the forces and moments due to the vehicle body and fixed surfaces plus the contributions from each of the flaps.[11–13]

$$C_\vartheta^B = C_\vartheta^R + C_\vartheta^{M_1} + C_\vartheta^{M_2} + C_\vartheta^{M_3} + C_\vartheta^{M_4} \tag{17}$$

Further, the forces and moments for any of the four flaps can be predicted from a model of a primary flap. Given this primary model with the total AoA, aerodynamic

bank, and deflection as variables, the other flaps' force and moment contributions are found by simply changing the aerodynamic bank or phase angle of the primary model shown as follows.[11,12]

$$C_N^{M_2}(\phi) = C_N^{M_1}\left(\phi + \frac{\pi}{2}\right), \qquad C_N^{M_3}(\phi) = C_N^{M_1}(\phi + \pi), \qquad (18)$$
$$C_N^{M_4}(\phi) = C_N^{M_1}(\phi + 3\pi/2)$$

The data set includes comprehensive sampling using the Missile DATCOM semi-empirical predictor, equally comprehensive sampling using the Cart3D inviscid CFD code, and sparse sampling using both the CFD++ NS CFD code and subscale wind tunnel tests. As the projectile has been widely studied, a full description of the computational data sources is found in Vasile et al.[5] Wind tunnel tests are described in Pokela et al.[6] Previous efforts at data fusion are described in Burchett et al.[7]

Previous efforts found polynomial coefficients for the following model:

$$C_\vartheta^R = C_{\vartheta 0}^R(M,\phi) + C_{\vartheta 1}^R(M,\phi)s_\alpha + C_{\vartheta 2}^R(M,\phi)s_\alpha^2 + C_{\vartheta 3}^R(M,\phi)s_\alpha^3 \qquad (19)$$
$$+C_{\vartheta 4}^R(M,\phi)s_\alpha^4 + C_{\vartheta 5}^R(M,\phi)s_\alpha^5$$

For body axial force, only the even powers were found. For axial moments, only the zeroth, first-, and second-order terms were found. For transverse force and moments, all terms of the fifth-order polynomial were found. This was done without any consideration of the amount of uncertainty in the resulting parameters ($C_{\vartheta i}^R$). In this report, we use the generalized least squares as shown previously to estimate the uncertainty in all parameters. Polynomial terms were then pruned from the model to limit the amount of uncertainty in terms, especially the linear ones.

5. Results Fixed Aerodynamic Surfaces

5.1 Cokriging

Sora's multi-fidelity cokriging utility will form a GP model from up to three multi-fidelity data sources at once.[8,9] Thus, we formed a model of the six forces and moments with Mach, AoA, and aerodynamic bank as the inputs using the lowest three fidelity sources (DATCOM, Cart3D, and CFD++). Then, we used the Sora tool in a recursive fashion by resampling the resulting model and cokriging it against the wind tunnel data.

Since the four-fin projectile has quarter-roll periodic symmetry, we need only to model the first 90° of aerodynamic bank, and this model can be replicated three times to represent a full roll cycle. The two lowest-fidelity data sources had the following input sampling.

$$M \in \{0.45,0.55,0.65, 0.75, 0.85, 0.95, 1.02, 1.2, 1.5, 2, 2.5, 3, 3.5, 4,6,9\}, N_M = 16$$
$$\alpha \in \{0°, 2°, 4°, \dots, 20°, 25°\}, N_\alpha = 12$$
$$\phi \in \{0°, 11.25°, 22.5°, \dots 78.75°, 90°\}, N_\phi = 9 \quad (20)$$

The last ϕ sample is redundant but helps to enforce the periodic symmetry in the GP models.

Next, we inquired the final cokriging (GP) model at the low-fidelity sampling while applying a finer grid in aerodynamic bank described by

$$\phi \in \{0°, 2.8125°, 5.625°, \dots 87.1875°, 90°\}, N_\phi = 33 \quad (21)$$

This finer grid will be used in the final set of polynomial coefficient tables and helps to illustrate uncertainty propagation in GP models.

Figure 2 shows the total force and moment predictions rendered by the final GP model at Mach = 2.5. Semi-transparent layers illustrate the 95% confidence interval on the predictions. Note that CFD++ and wind tunnel data were limited to 12° AoA, thus the uncertainty is greatly increased for large AoA. CFD++ included predictions at M = 2.5, but the wind tunnel included M = 1.2 and M = 5.0 with nothing in between. Thus, all the uncertainties are larger at this Mach number than for those in the wind tunnel data set.

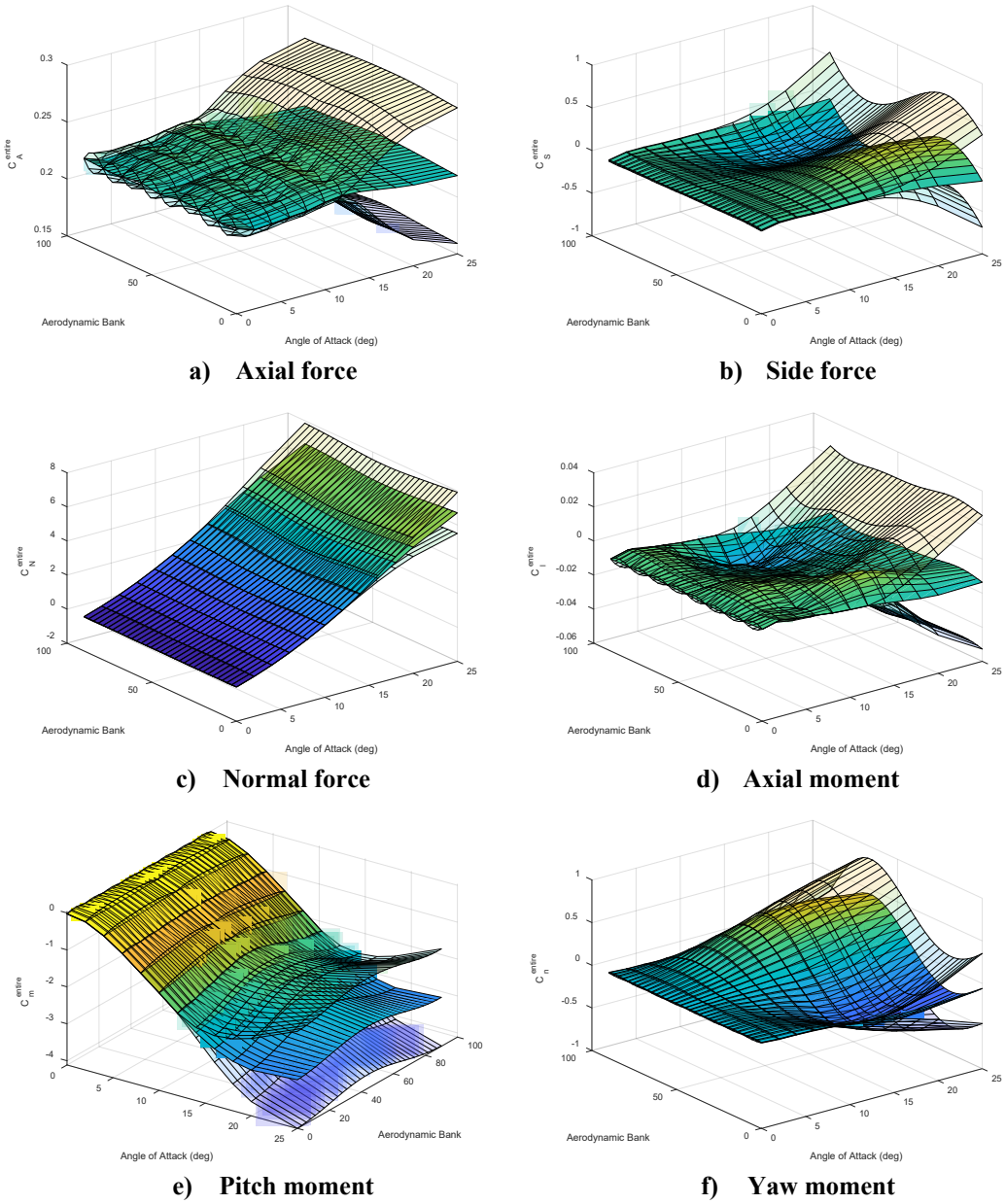

Fig. 2 Result of cokriging all four fidelities: M = 2.5. Semi-transparent surfaces depict the 95% confidence interval on all predictions.

To further illustrate the influence of high-fidelity anchor points on GP prediction uncertainty, we show slice plots in Figs. 3 and 4. Figure 3 is a slice of Fig. 2a along the AoA direction. Aerodynamic bank is held constant at 22.5° and Mach is 2.5. Note that this bank angle is not part of the wind tunnel sampling—AoA sweeps were performed at 0° and 45° of bank. Roll sweeps were performed at 0°, 6°, and 12° AoA. Thus the only wind tunnel anchor points for 22.5° of bank are at 0°, 6°, and 12° AoA. The plot clearly shows that the prediction uncertainty is extremely small at the anchor points. Uncertainty grows to about ±5% of the predicted values

at 3° and 9° AoA. The confidence interval becomes very large for high AoA, reaching about ±25% of the predicted mean at 25° AoA.

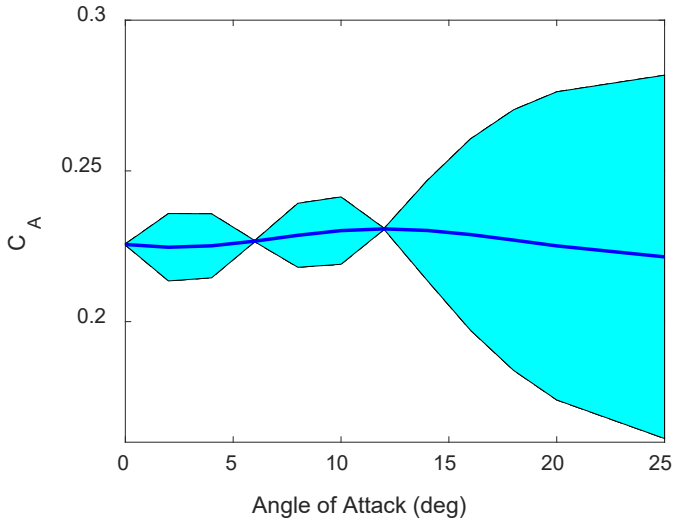

Fig. 3 Axial force prediction slice plot showing 95% confidence interval, M = 2.5, Φ = 22.5°

Figure 4 shows a slice of Fig 2a holding AoA constant at 6°. Mach is 2.5 and aerodynamic bank is swept from 0° to 90°. Since the wind tunnel data include a roll sweep at Mach 2.0, and 6° AoA, anchor points exist every 11.25° of roll. This is evident as the prediction uncertainty is very small at each 11.25° of roll. Prediction uncertainty grows to about ±7% between anchor points.

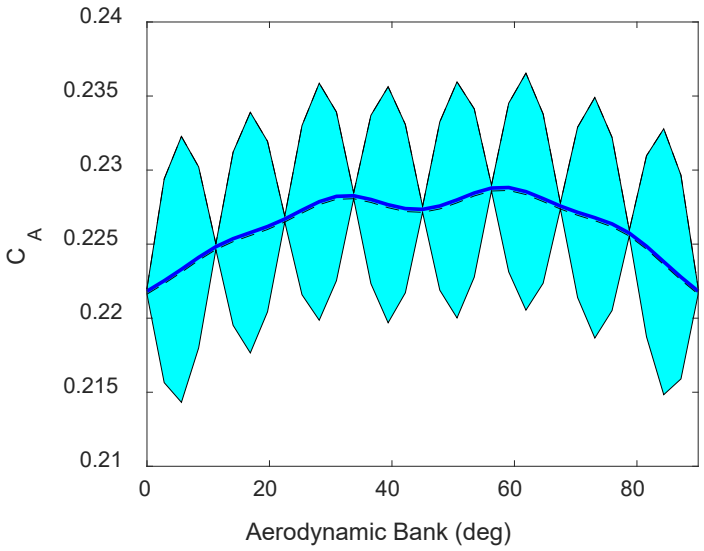

Fig. 4 Axial force prediction slice plot showing 95% confidence interval, M = 2.5, AoA = 6.0°

5.2 Regression

We used the multi-fidelity GP model to predict all six total force and moment components at the sampling described by

$$M \in \{0.45,0.55,0.65, 0.75, 0.85, 0.95, 1.02, 1.2, 1.5, 2, 2.5, 3, 3.5, 4,6,9\}, N_M = 16$$
$$\alpha \in \{0°, 2°, 4°, \dots, 20°, 25°\}, N_\alpha = 12$$
$$\phi \in \{0°, 2.8125°, 5.625°, \dots 87.1875°, 90°\}, N_\phi = 33 \quad (22)$$

Then, at every possible M, ϕ pair, we performed generalized regressions. After using the fifth-order polynomials described by Eq. 19, we realized that uncertainties were very high for the nonlinear terms, especially the even powers. To reduce uncertainty on all terms, but especially the linear ones, we explored reducing the polynomial order. Figure 5 illustrates this process.

Figure 5 shows the 2σ uncertainty in percent on three coefficients for a fourth-order polynomial and a fifth-order polynomial where even power terms are held at zero. In the top pane, uncertainties are roughly equal for the high-order term. In the middle pane, the quadratic coefficient of the fourth-order model has about three times the uncertainty as the cubic coefficient of the fifth order. In the bottom pane, the linear term of the fourth-order model has 10 times the uncertainty as that of the linear term of the three-term fifth-order model. Thus, we conclude that the full fifth-order model induces a great deal of uncertainty through overfitting. Eliminating the even power terms greatly reduces this uncertainty. We will fit fifth-order polynomials to the transverse force and moment predictions, holding the even power terms to zero.

Figure 6 depicts the result of polynomial regression for body *Z* force at Mach 2.5. The normal force predictions from the GP model are plotted as a surface. The GP model was used to interpolate every 2.8125° along the aerodynamic bank axis. We applied generalized least squares using the predictions and variances given by the GP model. This renders a set of fifth-order polynomial coefficients and their respective variances with the odd powers held at zero. Note from Fig. 2c that the prediction variance from the GP model is extremely small for AoAs of 12° or less. Variance increases greatly for 20° and 25° AoA. By using generalized least squares, we tell the regression not to trust predictions at high AoAs, but rather to precisely match predictions for 12° or less AoA. In Fig. 6, we juxtaposed predictions from the resulting polynomials as solid red lines with the surface of GP predictions. The polynomial for zero aerodynamic bank fits well at low AoA, but underpredicts the normal force at large AoA. This illustrates the trade-off in finding the best polynomial to fit the data in the most trusted region. Note that grid marks in AoA

are at each 2° increment. Most of the polynomials match the GP predictions well up to 16° AoA and almost all fit them well up to 14°.

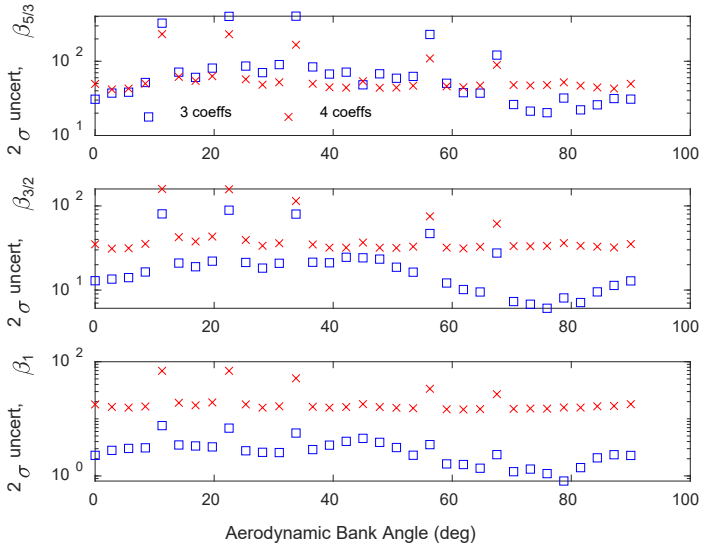

Fig. 5 Percent uncertainty comparison, M = 2.0. Red Xs depict the 2σ interval for β_3, β_2, and β_1 for a fourth-order polynomial regression. Blue squares depict the 2σ interval for β_5, β_3, and β_1 when β_4, β_2, and β_0 are held at zero in a fifth-order polynomial regression.

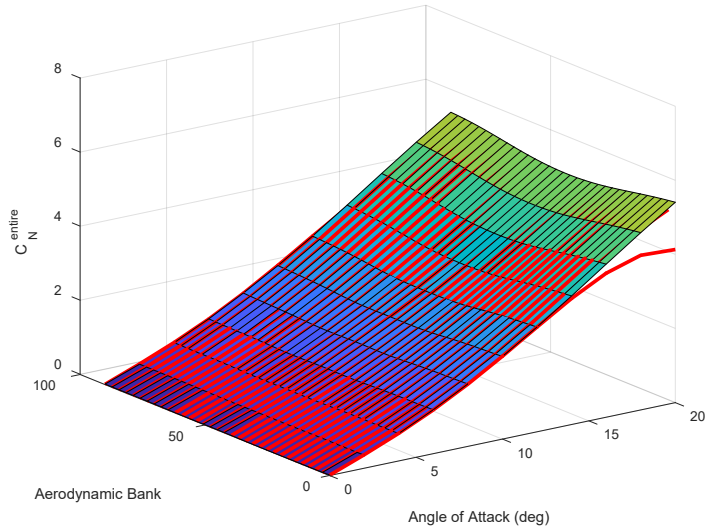

Fig. 6 Body *Z* force regression predictions plotted over cokriging total force predictions, M = 2.5

6. Results from Moving Aerodynamic Surfaces (MAS)

In this section, we describe the low- and high-fidelity data for the projectile with deflected flaps. We also present the results from cokriging. Since cokriging predicts model uncertainty, we use it to suggest conditions where the model would benefit greatly from additional high-fidelity measurements.

6.1 High-Fidelity Data from Wind Tunnel

Researchers at Florida State University captured total force and moment measurements for the projectile using a one-fifth subscale model with various configurations.[6] The cases with flap deflections were designed to model single-axis maneuvers by deflecting sets of flaps in symmetric ways. For example, roll maneuvers were simulated by deflecting all four flaps in equal amounts. Pitch maneuvers were designed in both the plus and X roll attitudes such that the pitch moment induced by the flap deflections would lie in the wind tunnel's horizontal axis. Specifically, pitch configurations in plus mode can be described by

$$\vec{\boldsymbol{\delta}} = \{\delta \quad 0 \quad -\delta \quad 0\}.$$

Pitch configurations in the X mode are described by

$$\vec{\boldsymbol{\delta}} = \{\delta \quad -\delta \quad -\delta \quad \delta\}.$$

Due to the time and cost required to capture wind tunnel data for a single configuration and flight condition, the overall set of data with deflections is the factorial of the following conditions: Mach $\in \{0.7, 2.0\}, \alpha \in \{0,2, \dots 12\}, \phi \in \{0°, 45°\}, \delta \in \{\pm 5°, \pm 10°, \pm 20°\}$, such that only plus mode configurations were tested at $\phi = 0°$ and only X mode configurations at $\phi = 45°$.

6.2 Low-Fidelity Data from Cart3D

Since the trailing-edge flaps of the projectile move independently, we seek a model that captures the force and moment contribution of a single flap over a wide range of conditions. Previous efforts determined a medium-fidelity model of an individual flap using an extensive CFD inquiry. Tens of thousands of predictions were made using Cart3D with a test grid described by set (20) replicated the requisite number of times to span the set of flap deflections described by set (23).[5]

$$\delta \in \{\pm 30°, \pm 25°, \pm 20°, \pm 15°, \pm 10°, \pm 5°, \pm 2°, 0°\} \qquad (23)$$

The resulting data set had many outliers that had to be eliminated by a multistep approach prior to use in data fusion.[14] The first step in the process included replacing points from obvious singularities with a linear interpolation from

neighboring points or replacing them directly from the corresponding point at a neighboring Mach number if linear interpolation failed. The second step was to fit a harmonic interpolating surrogate model along the aerodynamic roll direction for each slice of data with common deflection, Mach, and AoA. The final step was to form polynomial regressions for each output with AoA as the variable for each value of deflection, Mach, and aerodynamic bank. Burchett et al.[14] describes this process in detail.

Since the wind tunnel only captures the force and moment for the entire body, we built predictions at conditions described by sets (20) and (23) from the component models based on low-fidelity data. That is, rather than try to decompose the predictions from the wind tunnel into components, we decided to build up the entire body predictions from the low-fidelity surrogate.

The two bank attitudes tested in the wind tunnel have distinct configurations as shown in Section 6.1. Thus, we built a database for the entire body from the surrogate for the $\phi = 45°$ case (flaps deflected symmetrically as noted previously). We used the sampling described in sets (20) and (23) but limited Mach to ≤ 2.5 and $\alpha \leq 14°$.

6.3 Cokriging Results with Flap Deflections

We formed cokriging models of the transverse force and moment for the entire body in X mode with pitch deflections from the two data sources described previously.

Figure 7 shows the cokriging prediction of the pitch moment as a function of Mach and AoA for a deflection of $+20°$ at an aerodynamic bank of $0°$. The solid surface is the predicted mean. Semi-transparent surfaces depict the upper and lower bounds of the 95% confidence interval. Red asterisks represent the training data from Cart3D, and black diamonds depict the training data from the wind tunnel. Note that wind tunnel data only exists in two bands at Mach 0.7 and Mach 2.0. The cokriging algorithm treats the high-fidelity training data as "truth," so the confidence band shrinks to effectively ± 0 at each of the wind tunnel points. The confidence band grows in every direction away from the wind tunnel data so that it becomes quite large around Mach 1.35 and above Mach 2. It also becomes very large as AoA becomes large since no wind tunnel data exists for $\alpha > 12°$, and thus we limited the search space to $\alpha \leq 14°$.

The Cart3D predictions of the pitch moment are negative but smaller in magnitude than the wind tunnel measurements, especially at subsonic speeds. Thus, the wind tunnel found the vehicle more stable in pitch than expected from low-fidelity

surrogates. The cokriging model matches the wind tunnel data exactly and preserves the shape predicted by the low-fidelity data elsewhere. This makes cokriging an ideal method to fuse sparse anchor data with a dense grid of low-fidelity predictions. In this case specifically, the low-fidelity search grid includes 14 nonzero deflection cases and only six were tested in the wind tunnel. Other methods of interpolating between untested configurations seem dubious at best.

Figure 7 suggests that far more high-fidelity data is required to reduce uncertainty in the flap model predictions. In fact, for deflections that lack wind tunnel data, the prediction confidence bands grow to 100% of the prediction itself.

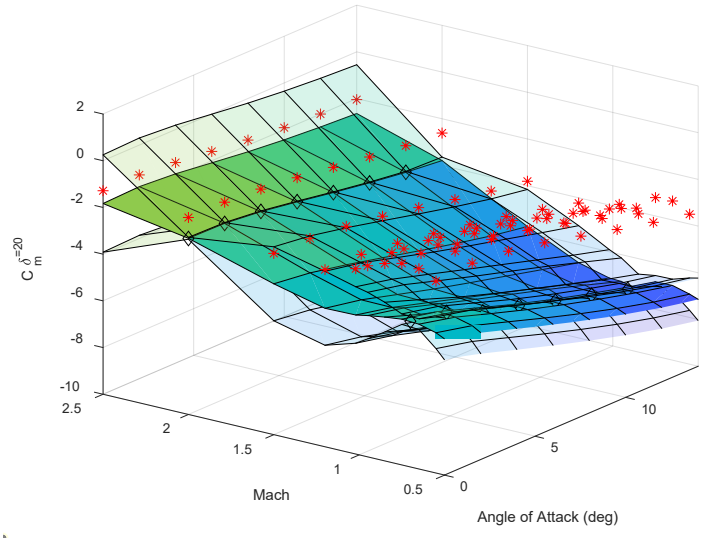

Fig. 7 Sample MAS cokriging result, δ = 20° ϕ = 0°

Figure 8 shows the low- and high-fidelity training data and cokriging model prediction for normal force for deflections that were tested in the wind tunnel. High- and low-fidelity data are shown as black diamonds and red asterisks, respectively. The cokriging prediction is shown as a solid surface for 0.5 < Mach < 2.5 and $0° \leq \alpha \leq 25°$.

Once again, cokriging preserved the shape of the surface formed by the low-fidelity data but shifts and rotates it in space to better match the high-fidelity data. Uncertainties are low where anchor data exists.

The cokriging model performance at configurations untested in the wind tunnel is shown in Fig. 9. Note that the cokriging surface still differs greatly from much of the low-fidelity training data. This shows that the cokriging model adjusts to anchor data for adjacent values of deflection. This is best illustrated in Figs. 9a and b. For the $\delta = -25°$ case, most of the low-fidelity data lies below the cokriging surface.

For $\delta = 15°$, the relationship is reversed. In the former case, the cokriging surface is pulled upward by the anchor data at $\delta = 20°$. In the latter, it has to form a smooth interpolant between the data at $\delta = 25°$ and the data at $\delta = 10°$.

The Appendix presents additional results including the normal force prediction in X mode, and the pitch moment and normal force predictions in plus mode.

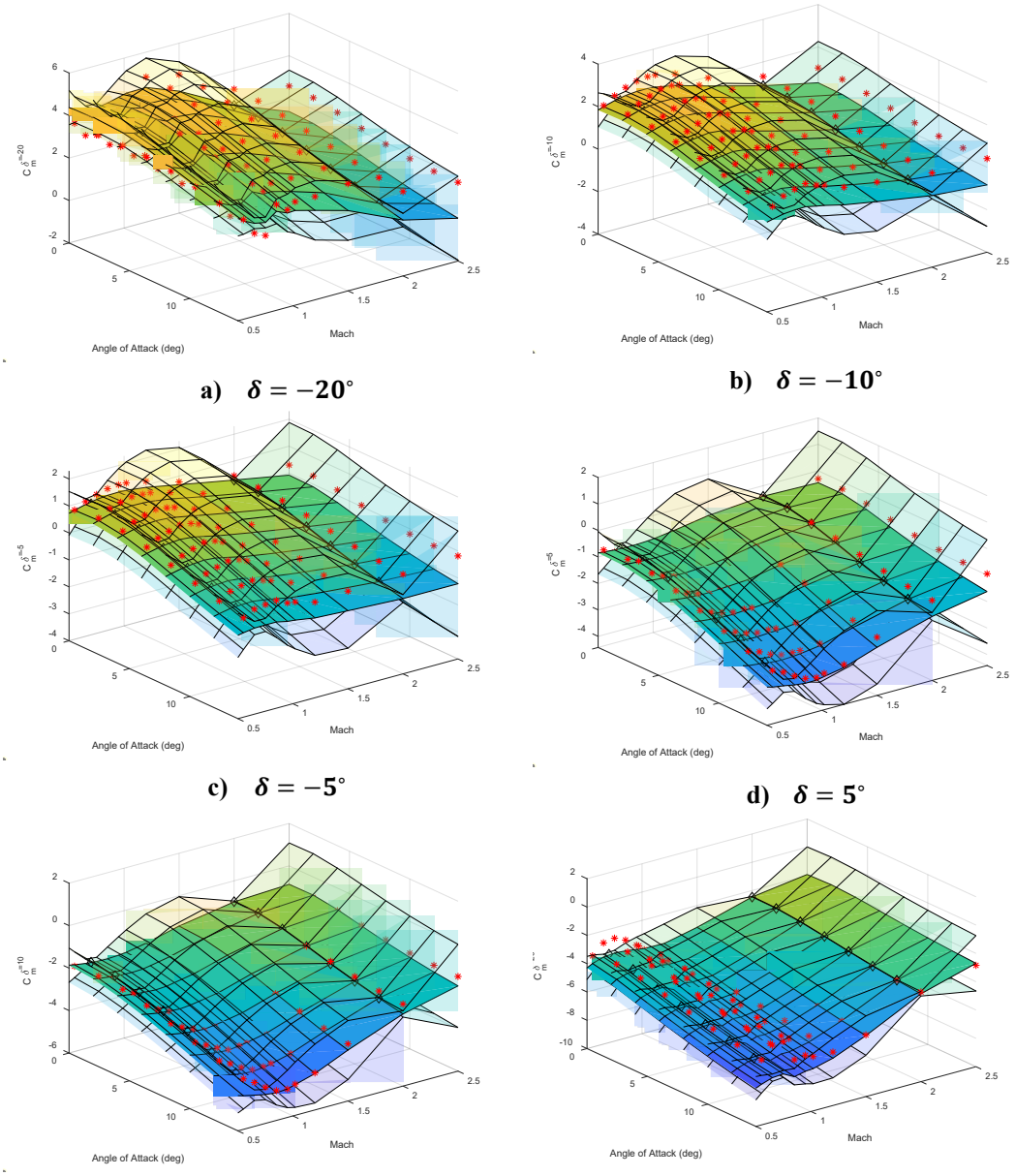

Fig. 8 Cokriging results for pitch moment. X mode configurations with deflections with anchor wind tunnel data.

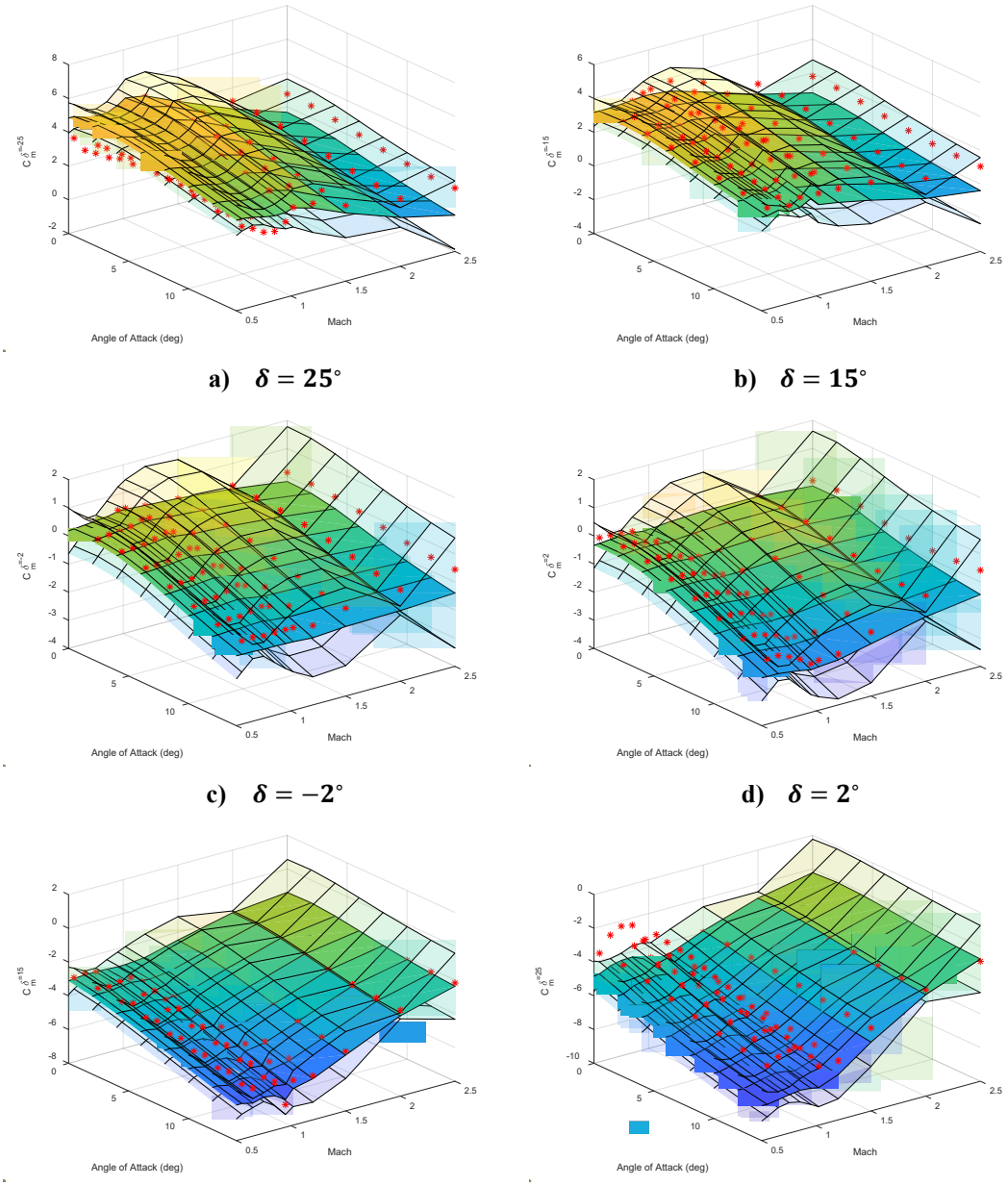

a) $\delta = 25°$ b) $\delta = 15°$

c) $\delta = -2°$ d) $\delta = 2°$

e) $\delta = 15°$ f) $\delta = 25°$

Fig. 9 Cokriging results for pitch moment. X mode configurations with deflections without anchor wind tunnel data.

6.4 Future Work

Now that cokriging models of transverse forces and moments have been formed, two additional steps are needed to acquire a tuned model of a single flap. First, the entire vehicle's predictions must be decomposed into rigid aerodynamic surface and moving aerodynamic surface components. Second, we need to perform general regression to convert the model to polynomial coefficients with variable AoAs and eliminate AoA from table lookups.

The process of this section should also be applied for roll configurations as wind tunnel data is available for roll—all flaps deflected equally—as well.

7. Conclusion

Aerodynamicists often glean force and moment predictions from several models and experiments of varying fidelity. A key challenge is how to combine the various sets of data in an optimal way. Cokriging or multi-fidelity GP modeling is a method that meets this challenge. This report shows how cokriging can be used in conjunction with generalized regression to determine the uncertainty of aerodynamic coefficient estimates.

Two models were formed for the projectile. The first model predicts forces and moments with no flap deflections. We demonstrated generalized regression for this case and noted that coefficient uncertainty is reduced by ignoring even power terms. The second model predicts forces and moments on the vehicle with flaps deflected symmetrically for pitch motion. Additional work remains to decouple the contribution of a single flap and find its force/moment model as polynomials in AoA.

8. References

1. Krige DG. A statistical approach to some basic mine valuation problems in the Witwatersrand. J South Afr Inst Min Metall. 1951;52(6):119–139.

2. Forrester AIJ, Sobester A, Keane AJ. Multi-fidelity optimization via surrogate modeling. Proc R Soc Lond A Math Phys Sci. 2007;463(2088):3251–3269.

3. Bailly J, Bailly D. Multifidelity aerodynamic optimization of a helicopter rotor blade. AIAA J. 2019;57(8):3132–3144.

4. Lawless ZD, Dreyer ER, Smith CA. CFD-based kriging surrogate models compared to axisymmetric missile concept from Mach 0.60 to 3.95. AIAA SciTech Forum; 2023 Jan 23–27; National Harbor, MD. doi:10.2514/6.2023-2278.

5. Vasile J, Bryson J, Sahu J, Paul J, Gruenwald B. Aerodynamic dataset generation of a long-range projectile. DEVCOM Army Research Laboratory (US); 2020 Aug. Report No.: ARL-TR-9019.

6. Pokela RC, Kumar R, Vasile JD. Experimental and computational aerodynamic characterization of a generic high-speed projectile configuration. AIAA Aviation 2021 Forum; 2021 Aug 2–6. doi.org/10.2514/6.2021-2607

7. Burchett B, Vasile J, Bryson J. Combining sparse and dense databases to form a robust aerodynamic model for a long-range high-speed projectile. DEVCOM Army Research Laboratory (US); 2021 July. Report No.: ARL-TR-9235.

8. Quinlan KR, Movva J, Burchett BT, Vasile JD, Driver D, Acton J. Evaluation of multi-fidelity approaches with active learning for automated database generation. AIAA Aviation 2023 Forum; 2023 June 12–16; San Diego, CA. doi.org/10.2514/6.2023-4023

9. Lawrence Livermore National Laboratory. Sora user manual. Flight Performance Integration LLNL Analysis Group; 2022 Mar 1. Report No.: LLNL-SM-838736.

10. Strang G. Introduction to applied mathematics. Wellesley-Cambridge Press; 1986.

11. Vasile J, Bryson J, Sahu J, Paul J, Gruenwald B. Aerodynamic dataset generation of a long range projectile. DEVCOM Army Research Laboratory (US); 2020 Aug. Report No.: ARL-TR-9019.

12. Vasile JD, Sahu J. Roll Orientation-dependent aerodynamics of a long-range projectile. DEVCOM Army Research Laboratory (US); 2020 Aug. Report No.: ARL-TR-9017.

13. Heeg J. Control Surface interaction effects of the Active Aeroelastic Wing wind tunnel model. 47th AIAA/ASME/ASCE/AHS/ACS Structures, Structural Dynamics, and Materials Conference; 2006 May 1–4; Newport, RI.

14. Burchett BT, Paul JL, Vasile JD, Bryson JT. A high-fidelity, roll-dependent aerodynamic model for a long-range, high-speed missile. DEVCOM Army Research Laboratory (US); 2021 July. Report No.: ARL-TR-9236.

Appendix. Additional Results

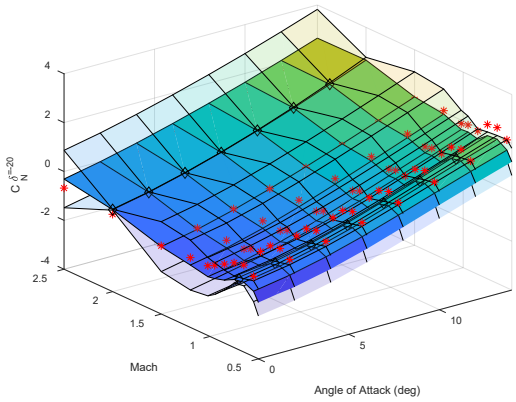

a) $\delta = -20°$

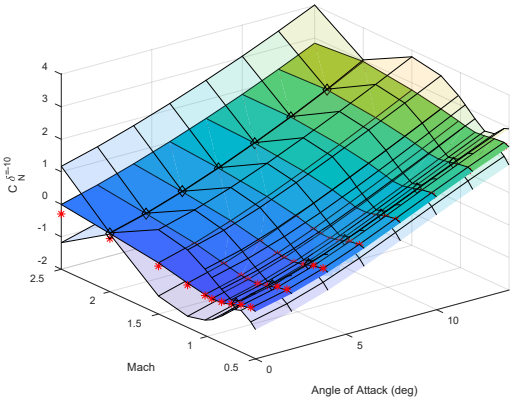

b) $\delta = -10°$

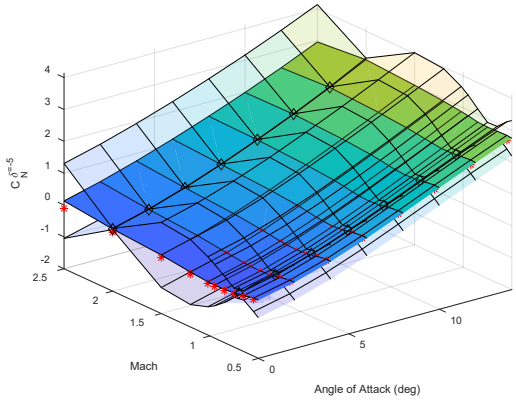

c) $\delta = -5°$

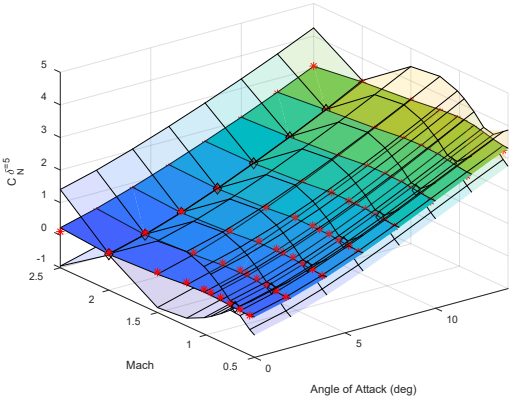

d) $\delta = 5°$

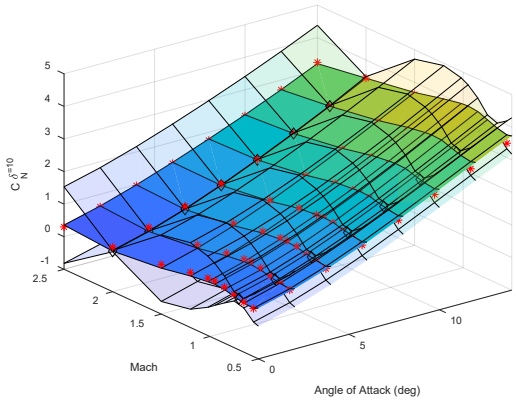

e) $\delta = 10°$

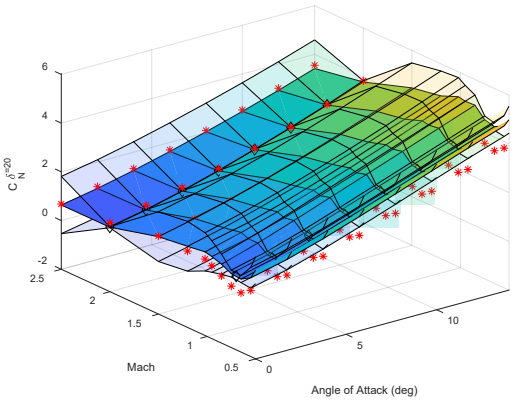

f) $\delta = 20°$

Fig. A-1 Cokriging results for normal force. X mode configurations with deflections with anchor wind tunnel data.

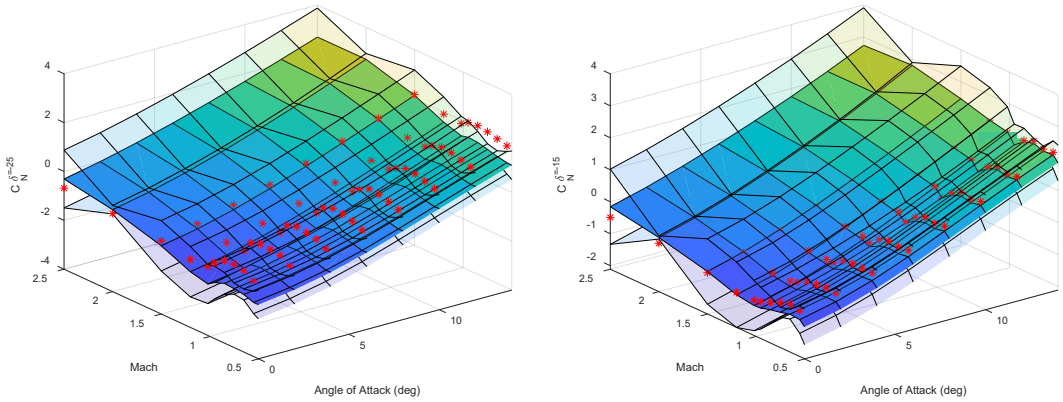

a) $\delta = -25°$ b) $\delta = -15°$

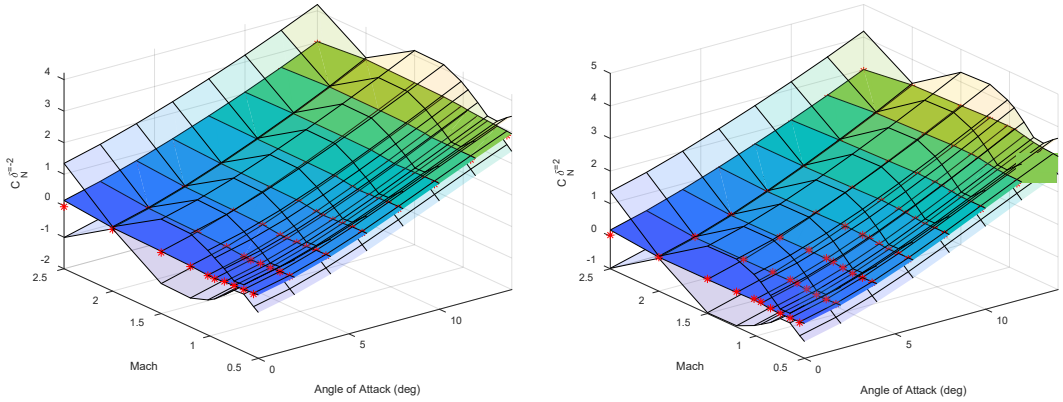

c) $\delta = -2°$ d) $\delta = 2°$

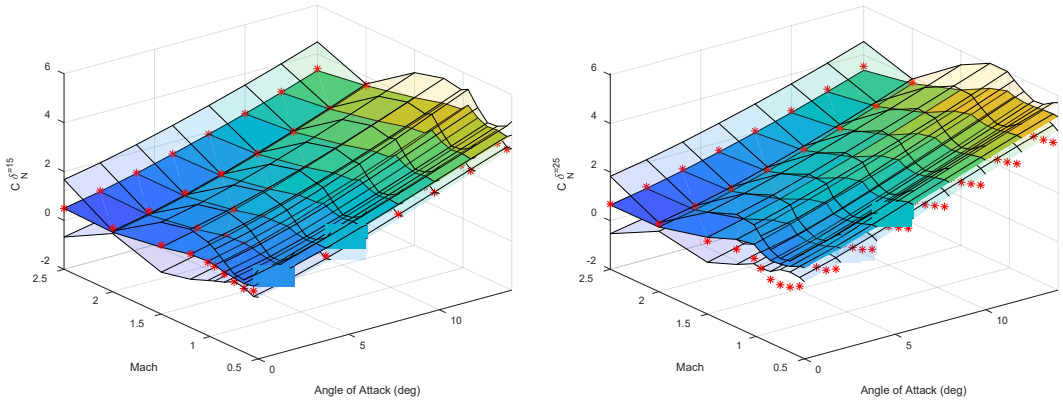

e) $\delta = 15°$ f) $\delta = 25°$

Fig. A-2 Cokriging results for normal force. X mode configurations with deflections without anchor wind tunnel data.

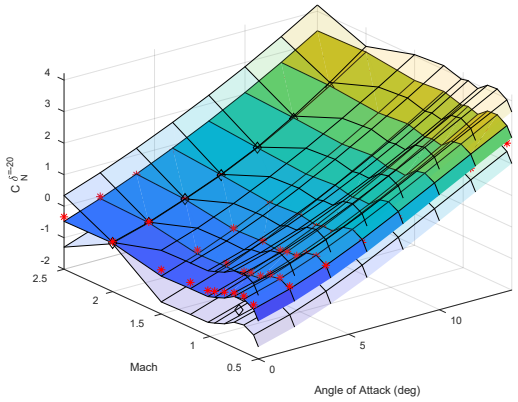

a) $\delta = -20°$

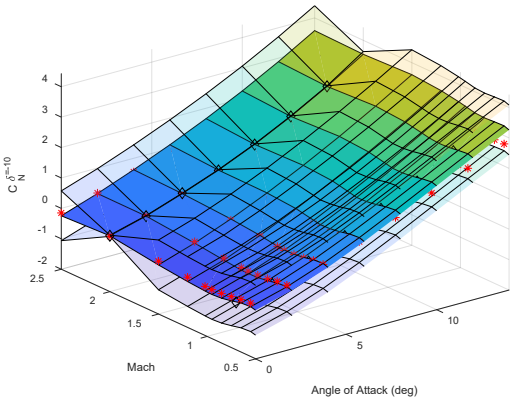

b) $\delta = -10°$

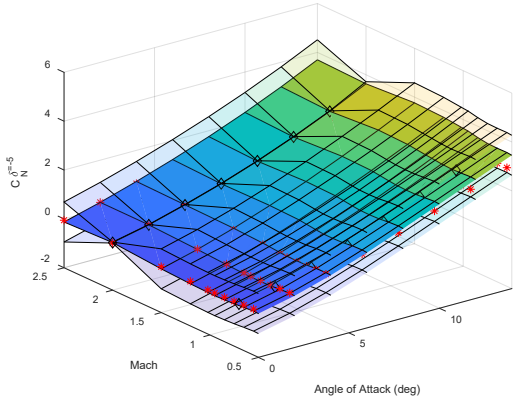

c) $\delta = -5°$

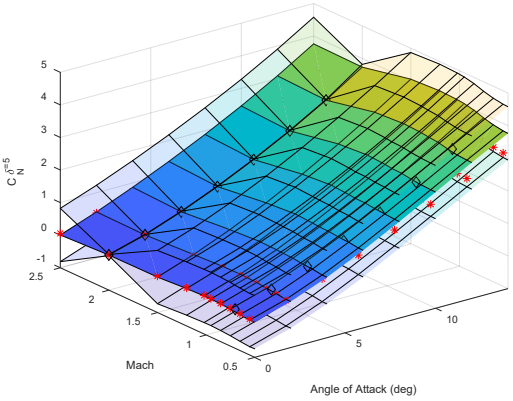

d) $\delta = 5°$

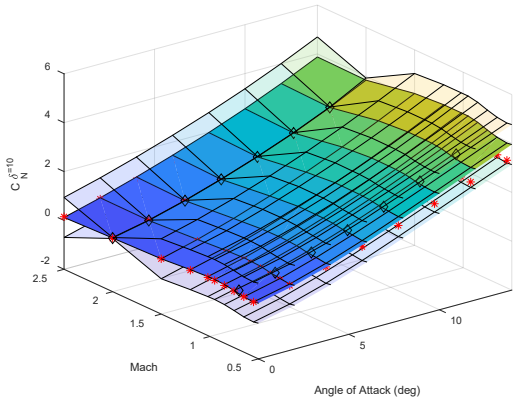

e) 10

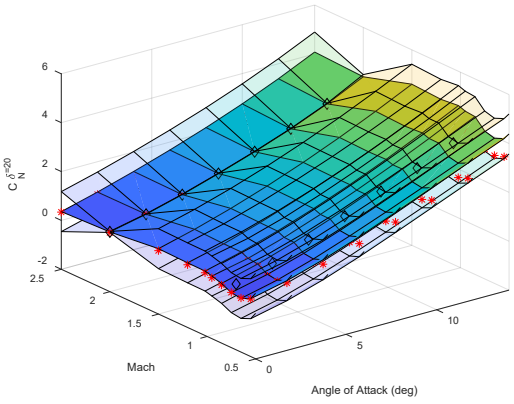

f) 20

Fig. A-3 Cokriging results for normal force. Plus mode configurations with deflections with anchor wind tunnel data.

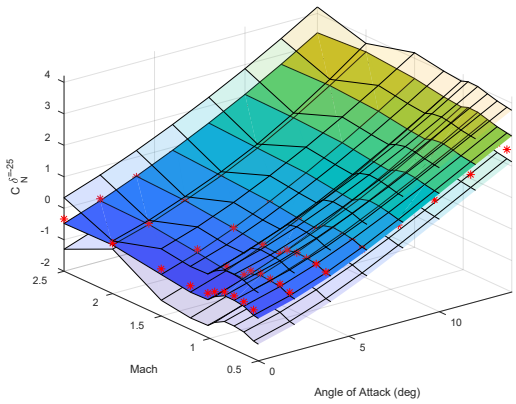

a) $\boldsymbol{\delta = -25^{\circ}}$

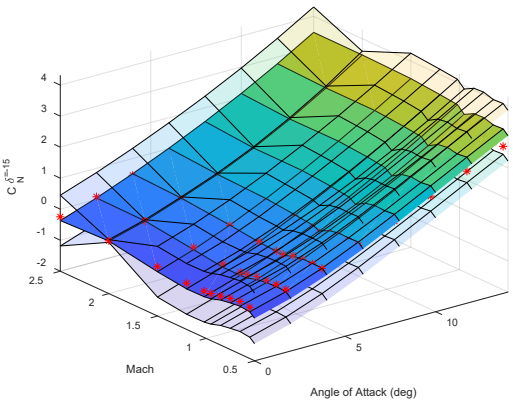

b) $\boldsymbol{\delta = -15^{\circ}}$

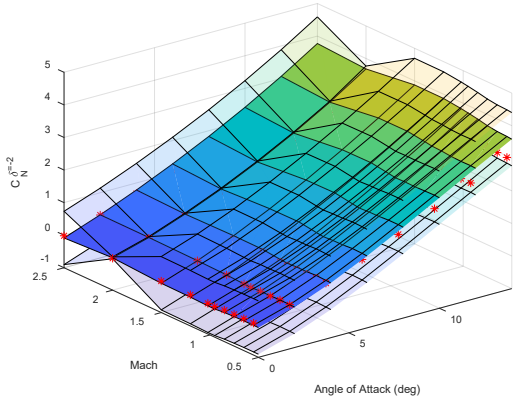

c) $\boldsymbol{\delta = -2^{\circ}}$

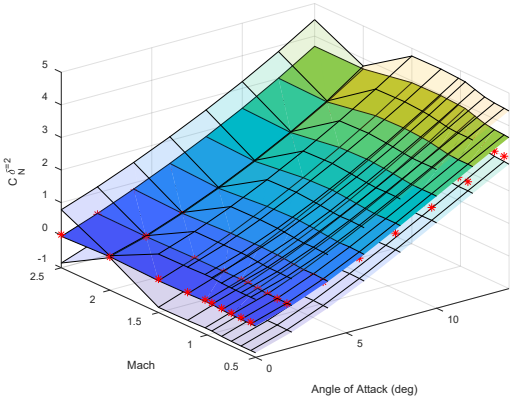

d) $\boldsymbol{\delta = 2^{\circ}}$

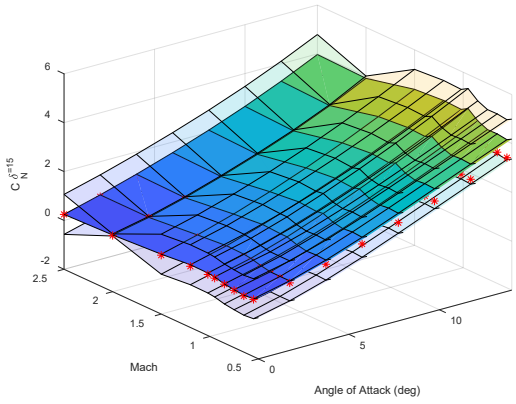

e) $\boldsymbol{\delta = 15^{\circ}}$

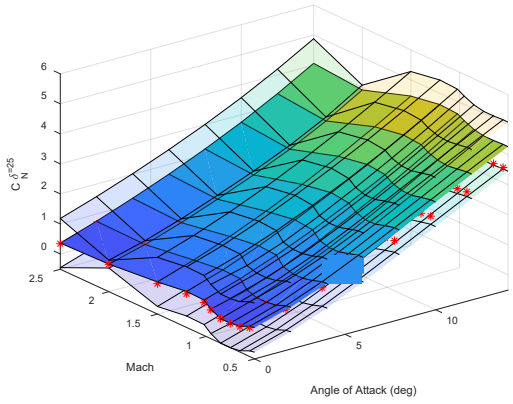

f) $\boldsymbol{\delta = 25^{\circ}}$

Fig. A-4 Cokriging results for normal force. Plus mode configurations with deflections without anchor wind tunnel data.

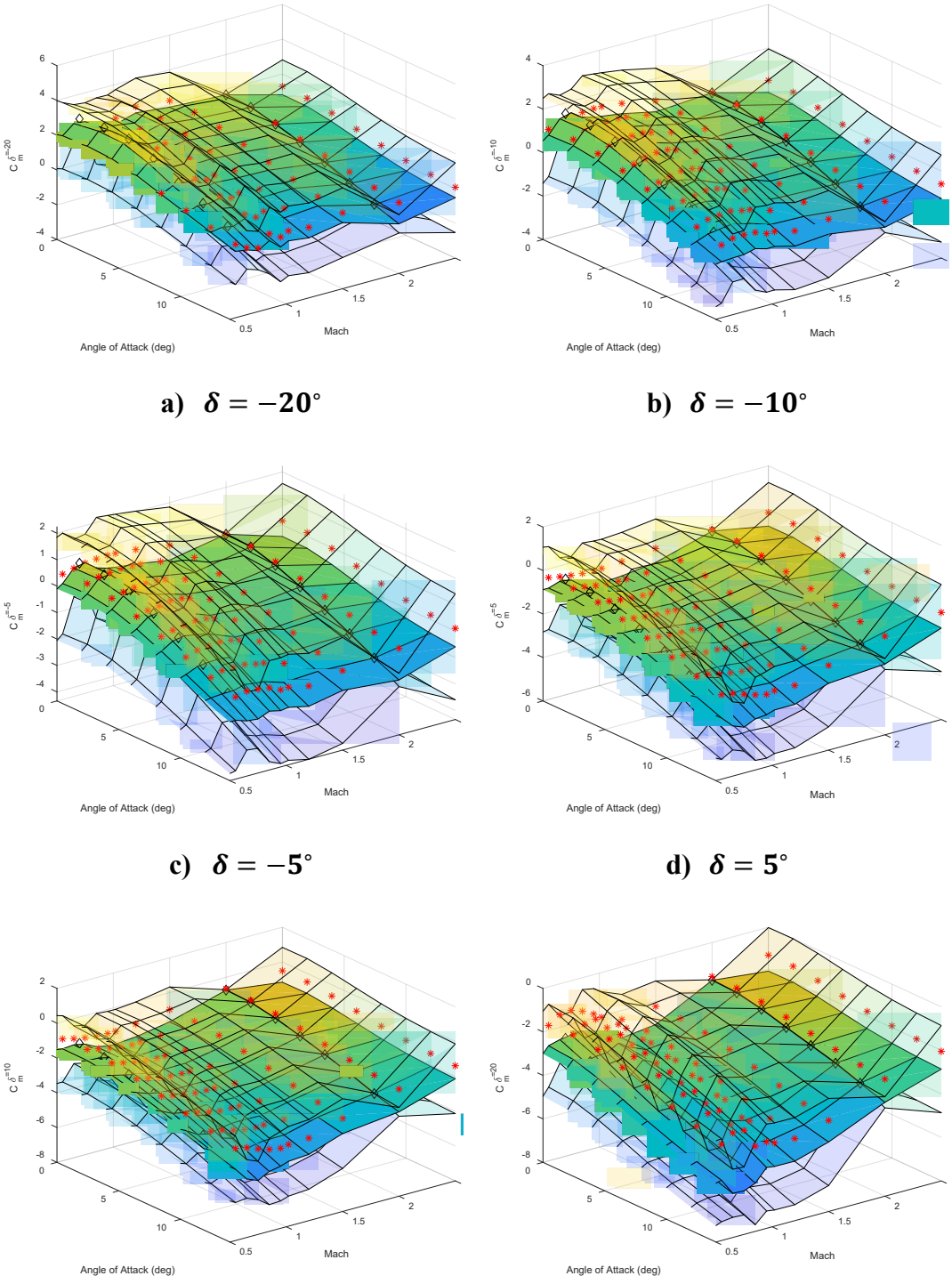

a) $\delta = -20°$ **b)** $\delta = -10°$

c) $\delta = -5°$ **d)** $\delta = 5°$

e) **10** **f)** **20**

Fig. A-5 Cokriging results for pitch moment. Plus mode configurations with deflections with anchor wind tunnel data.

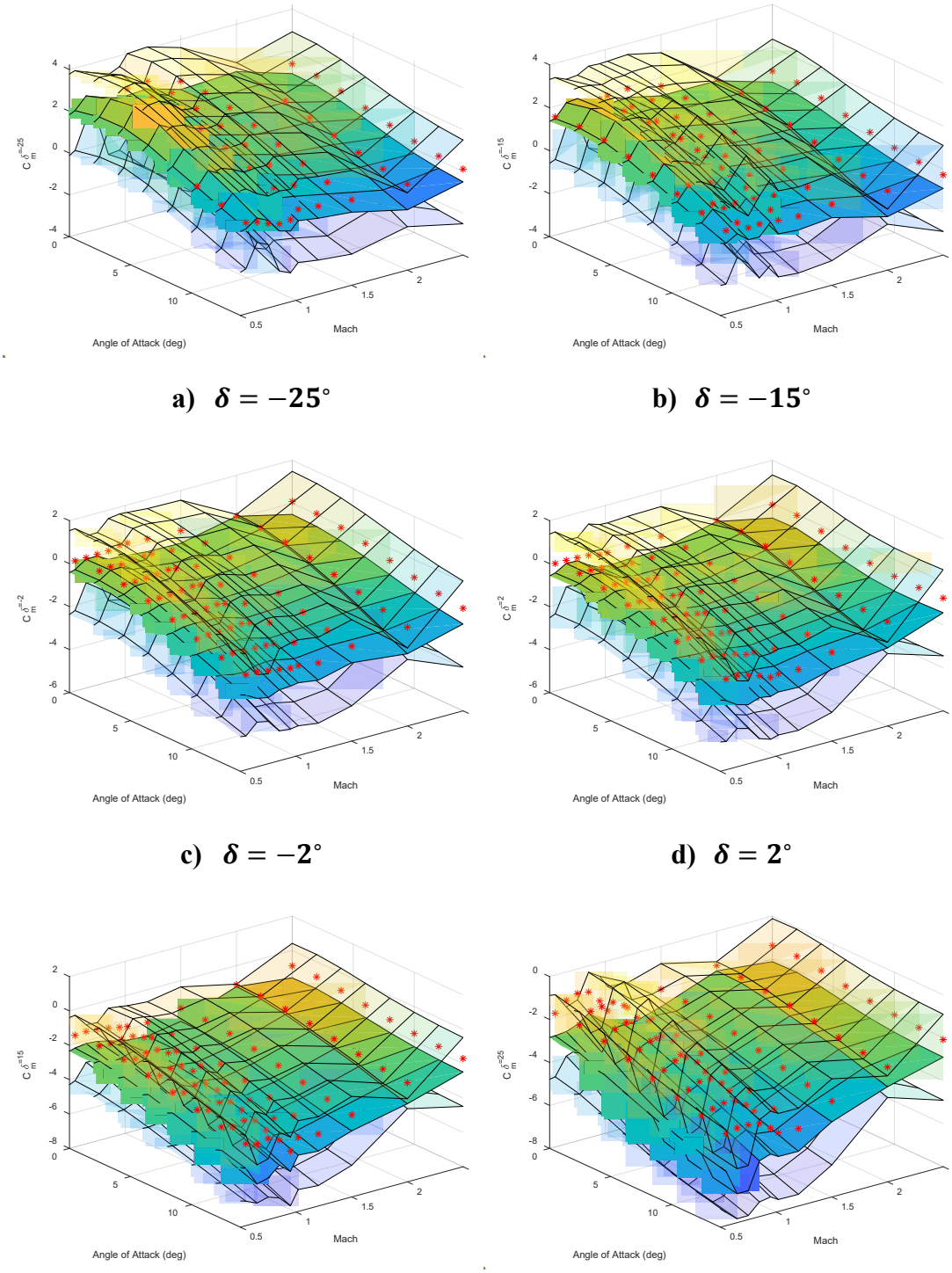

a) $\delta = -25°$

b) $\delta = -15°$

c) $\delta = -2°$

d) $\delta = 2°$

e) $\delta = -15°$

f) $\delta = -25°$

Fig. A-6 Cokriging results for pitch moment. Plus mode configurations with deflections without anchor wind tunnel data.

List of Symbols, Abbreviations, and Acronyms

3-D	three-dimensional
AOA	angle of attack
ARL	Army Research Laboratory
CFD	computational fluid dynamics
DEVCOM	US Army Combat Capabilities Development Command
GP	Gaussian process
MAS	moving aerodynamic surfaces
NS	Navier–Stokes
C_{ϑ}^{R}	aerodynamic coefficient ϑ for rigid aero surfaces
$C_{\vartheta}^{M_i}$	aerodynamic coefficient ϑ for flap i
$C_{m}^{\delta=x}$	total pitch moment coefficient with symmetric $\delta = x$
$C_{N}^{\delta=x}$	total normal force coefficient with symmetric $\delta = x$
α	angle of attack (degrees)
M	Mach number
ϕ	aerodynamic bank angle (degrees)
δ	flap deflection (degrees)
s_{α}	$\sin(\alpha)$
Subscript	
m	pitch moment
y	body side (y) force
N	body normal (-Z) force
0	zero AOA term
Superscript	
T	matrix transpose

1 (PDF) DEFENSE TECHNICAL INFORMATION CTR DTIC OCA

1 (PDF) DEVCOM ARL FCDD RLB CI TECH LIB

3 (PDF) DEVCOM AVMC FCDD AMS MMA P CROSS M MCDANIEL R OPPENHEIM

10 (PDF) DEVCOM ARL FCDD RLA WD L STROHM VA BHAGWANDIN J BRYSON B BURCHETT I CELMINS J DESPIRITO LD FAIRFAX B GRUENWALD J PAUL JD VASILE

3 (PDF) LAWRENCE LIVERMORE NAT'L LAB FLIGHT PERFORMANCE INTEGRATION J ACTON D DRIVER J MOVVA